

Distinct Speed and Direction Memories of Migrating Dendritic Cells Diversify Their Search Strategies

M. Reza Shaebani,^{1,2,*} Matthieu Piel,³ and Franziska Lautenschläger^{2,4}

¹*Department of Theoretical Physics, Saarland University, 66123 Saarbrücken, Germany*

²*Centre for Biophysics, Saarland University, 66123 Saarbrücken, Germany*

³*Institut Curie and Institut Pierre Gilles de Gennes,*

PSL Research University, CNRS, UMR 144, Paris, France

⁴*Department of Experimental Physics, Saarland University, 66123 Saarbrücken, Germany*

ABSTRACT Migrating cells exhibit various motility patterns, resulting from different migration mechanisms, cell properties, or cell-environment interactions. The complexity of cell dynamics is reflected, e.g., in the diversity of the observed forms of velocity autocorrelation function— that has been widely served as a measure of diffusivity and spreading. By analyzing the dynamics of migrating dendritic cells *in vitro*, we disentangle the contributions of direction θ and speed v ($\equiv |v|$) to the velocity autocorrelation. We find that the ability of cells to maintain their speed or direction of motion is unequal, reflected in different temporal decays of speed and direction autocorrelation functions, $\mathcal{AC}_v(t) \sim t^{-1.2}$ and $\mathcal{AC}_\theta(t) \sim t^{-0.5}$, respectively. The larger power-law exponent of $\mathcal{AC}_v(t)$ indicates that the cells lose their speed memory considerably faster than the direction memory. Using numerical simulations, we investigate the influence of \mathcal{AC}_θ and \mathcal{AC}_v as well as the direction-speed cross-correlation $\mathcal{C}_{\theta-v}$ on the search time of a persistent random walker to find a randomly located target in confinement. Although \mathcal{AC}_θ and $\mathcal{C}_{\theta-v}$ play the major roles, we find that the speed autocorrelation \mathcal{AC}_v can be also tuned to minimize the search time. Adopting an optimal \mathcal{AC}_v can reduce the search time even up to 10% compared to uncorrelated spontaneous speeds. Our results suggest that migrating cells can improve their search efficiency, especially in crowded environments, through the directional or speed persistence or the speed-direction correlation.

SIGNIFICANCE Various biological processes rely on the ability of cells to migrate. Of particular interest is the immune response, which crucially depends on the efficiency of finding harmful pathogens by migrating immune cells. By studying the *in vitro* dynamics of dendritic immune cells, we observe that the local directional change and instantaneous speed of the cell are cross-correlated to each other. However, the speed autocorrelation of the cell decays faster than its direction autocorrelation. Our numerical simulations of a correlated persistent search to find a randomly located target in confinement reveal that optimal search strategies can be achieved by minimizing the search time with respect to the speed or direction memory or the degree of speed-direction coupling.

INTRODUCTION

The ability of cells to migrate through crowded and confined spaces is crucial for various biological processes such as the immune response, brain development, and tumor spreading [1–4]. To obtain more insight into the underlying mechanisms of cell migration, the dynamics of cells have been extensively studied in recent years [5–15]. Migrating cells are active biological agents, which— similar to other living matter such as bacteria [16] and molecular motors [17–19]— exhibit anomalous diffusive dynamics over a wide range of length and time scales [20]; this is manifested, e.g., in non-Gaussian probability distributions of speed or position [5–8, 21–25], crossovers between different anomalous diffusion regimes [5, 8, 9, 21–23], and slow decay of velocity correlation functions [5, 6, 9, 21–24]. Many factors have been identified to influence the cell dynamics, including the mechanical properties and type of the cell, being a normal or abnormal cell, dimen-

sionality, presence of environmental cues, and cell interactions with other cells, substrate, or confining boundaries. As a result, various mathematical approaches have been proposed to capture the cell dynamics, ranging from generalized Langevin equation and fractional diffusion equations with temporal memory [6, 21] to Lévy walks [9, 10] and persistent random walk models [26].

Since a full mathematical description of the cell migration process is challenging in general, often informative concepts— such as the velocity autocorrelation function (VAF)— have been employed to describe the cell dynamics. VAF carries useful information about the path memory and diffusivity of the moving (biological) agent, which affect its transport, taxis, and search efficiency [27–29]. Nevertheless, the complexity of cell dynamics affects the behavior of VAF as well; various forms of VAF have been reported for migrating cells. This includes an exponential decay in *Dictyostelium* (Dicty) and neural stem cells [7, 11], a sum of two exponentials in keratinocytes, fibroblasts, Dicty, and brain cancer cells [12, 22, 24], a slower than exponentially in fibrosarcoma, breast cancer, and T cells [5, 6, 9], and a power-law tail decay in Hydra

* Corresponding author. Email: shaebani@lusi.uni-sb.de.

and epithelial cells [21, 23]. For comparison, the temporal decay of the VAF in a persistent random walk follows an exponential form [30]; however, long-range temporal correlations or memory effects lead to non-exponential forms [6, 31] (with a faster or slower than exponential tail, depending on the choice of the memory kernel [31]).

The VAF contains the combined memories of instantaneous directions θ and speeds v of the cell. The question arises as to whether a migrating cell necessarily carries the same temporal memories of directional and speed changes. There have been evidences that the directional persistence and instantaneous speed are cross-correlated in various types of migrating cells [5, 13–15, 32–35]; a larger speed strengthens the retrograde actin flows and stabilizes the cell polarization by enhancing the asymmetry of the concentration profile of polarity cues [13]. However, the strength of the cross-correlation $C_{\theta-v}$ between the instantaneous θ and v varies from cell to cell, is always smaller than 1 (i.e. weaker than a linear relation), and weakens with increasing v ; the degree of coupling is the strongest at small values of v and gradually decays to zero (i.e. an uncorrelated θ and v) at high v [13, 14]. This suggests that the temporal autocorrelation functions of directions $\mathcal{AC}_\theta(t)$ and speeds $\mathcal{AC}_v(t)$ may display different statistics.

Achieving an efficient transport and navigation is crucial for migrating cells in general, and for immune cells in particular, since they are responsible to explore the environment in search for harmful pathogens. While efficient search strategies have been identified in various biological systems [29, 36–40], the optimality of search and navigation in cell migration processes remains much less studied and understood. For a persistent random search in confinement with a constant speed, it was shown that adopting an optimal (confinement-size dependent) directional persistence minimizes the search time [41]. The directional persistence can be characterized, e.g., by the mean length or time during which the searcher maintains its direction of motion. Alternatively, the temporal autocorrelation function $\mathcal{AC}_\theta(t)$ of instantaneous directions θ carries similar information. The characteristic decay time t_θ of $\mathcal{AC}_\theta(t)$ can be served as a measure of directional persistence. The mean search time when moving with the optimal directional persistence t_θ^{opt} can be even less than a half of the search time for a non-persistent motion, depending on the size of the confinement [14, 41]. Indeed, moving with the optimal directional memory t_θ^{opt} at a constant speed results in the absolute minimum of the search time; but moving with a desired persistence is often unfeasible in crowded biological environments. Moreover, migrating cells experience considerable speed variations. When moving with a variable speed and a mean directional persistence smaller than t_θ^{opt} in a crowded environment, it has been proven [14] that inducing a cross-correlation $C_{\theta-v}$ between instantaneous speed v and direction θ (as observed for migrating cells) improves the search efficiency. Nevertheless, the benefit of cells from this strategy is rather limited since they can

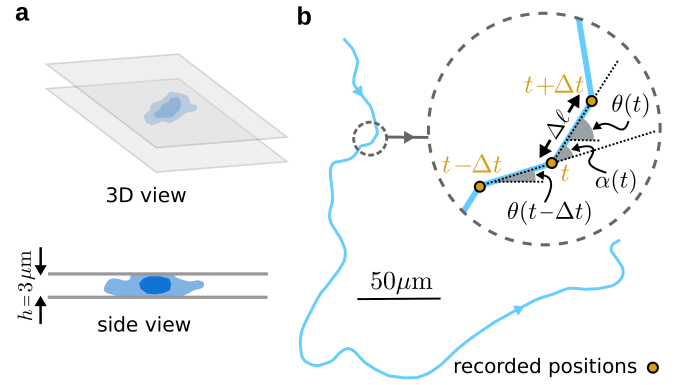


FIG. 1. (a) Schematic drawings of the experimental setup. (b) Sketch of a sample cell trajectory. The local direction of motion $\theta(t)$ and the local turning-angle $\alpha(t)$ are depicted. From the local displacement $\Delta\ell$, the instantaneous speed is obtained as $v(t) = \Delta\ell / \Delta t$.

maintain the θ - v coupling only up to moderate values of v . It is unclear whether there are alternative possibilities for cells to reduce their search time.

We perform *in vitro* experiments of dendritic immune cell migration in quasi two-dimensional confinements (Fig. 1a). By analyzing the kinematics of the cells from their trajectories, we separate the contributions of direction and speed to the VAF and verify that the separated speed and direction autocorrelation functions, \mathcal{AC}_v and \mathcal{AC}_θ , carry useful information about the cell dynamics, that cannot be directly read from the VAF itself. We show that the cells carry unequal memories of successive speeds or directions; the decay of the speed memory is considerably faster than the directional one. By performing extensive Monte Carlo simulations, we investigate the search process in a general correlated random walk consisting of autocorrelated speeds and/or orientations that are cross-correlated to each other as well. We isolate the roles of \mathcal{AC}_θ , \mathcal{AC}_v , and $C_{\theta-v}$, and verify that, besides other strategies, smooth variations of speed can help the searcher to optimize its search for randomly located targets.

MATERIALS AND METHODS

Cell migration experiments

We study the dynamics of Murine bone marrow-derived immature dendritic cells *in vitro*. The cells are confined between the cell culture dish and a ceiling held by microfabricated pillars made out of Polydimethylsiloxane (PDMS) as described in [42]. The confinement height is $3 \mu\text{m}$; see Fig. 1a. To prevent cell-surface adhesion and exclude migration in mesenchymal mode, both surfaces are coated with a non-adhesive material (PLL-PEG; 0.5 mg/mL). The cells are highly squeezed between the parallel plates because in the absence of adhesion, they have a nearly spherical shape when lying on a plate, with an average height of $\approx 11 \mu\text{m}$ [43]. We note that the height of these cells can be smaller [44, 45], e.g. when using other

coatings— since a different coating can allow for cell-surface adhesion to some extent, which stretches the cell along the surface. Cell nuclei are stained with Hoechst 34580 (200 ng/mL for 30 min) (Sigma Aldrich, St Louis, USA) and the cell trajectories are recorded by epifluorescence microscopy for about 6h at 37°. The sampling rate and pixel size of the camera have been 20 frames/h and 6.5 μm , respectively. To be able to treat the cells as non-interacting, we choose a low enough cell concentration.

Data analysis

We analyze cell trajectories with ImageJ plugin TrackMate. Each trajectory consists of a set of (x, y) positions, recorded after successive time intervals $\Delta t = 3$ min. We note that while a higher frame rate of the camera leads to a more accurate cell tracking, it can cause damage to cells due to light intensity. Additionally, a too high temporal resolution leads to a noisy track as the quality of tracking is technically limited and also because the changes in cell shape (that are not a real cell displacement) affect the localisation of the cell center. The chosen value of Δt enables us to record the successive cell positions with a resolution around the cell size itself, which has been accurate enough for our purposes. The instantaneous velocity \mathbf{v} and the local direction of motion θ are calculated from each pair of successive recorded positions (see Fig. 1b). The local turning-angle α is extracted from three successive recorded positions, from which the turning-angle distribution $F(\alpha)$ is constructed. For a highly persistent or antipersistent motion, $F(\alpha)$ develops a peak around $\alpha = 0$ or π , respectively [46]. We filter the trajectories with instantaneous speeds larger than 30 or smaller than 0.05 $\mu\text{m}/\text{min}$ to exclude image processing artifacts and immobile cells. The velocity autocorrelation function is calculated as $\text{VAF}(t) = \langle \mathbf{v}(t_0) \cdot \mathbf{v}(t_0 + t) \rangle / \sigma_v^2$, with $\langle \dots \rangle$ denoting the temporal and ensemble average over all the trajectories and σ_v^2 being the speed variance. Similarly, the autocorrelation functions of instantaneous speeds and directions are obtained as $\mathcal{AC}_v(t) = \langle (v(t_0 + t) - \bar{v})(v(t_0) - \bar{v}) \rangle / \sigma_v^2$ and $\mathcal{AC}_\theta(t) = \langle (\theta(t_0 + t) - \bar{\theta})(\theta(t_0) - \bar{\theta}) \rangle / \sigma_\theta^2$, with v being the speed, i.e. $v(t) = \sqrt{v_x^2(t) + v_y^2(t)}$. The cross-correlation between instantaneous speed and direction is calculated as $\mathcal{C}_{\theta-v} = \langle (\theta - \bar{\theta})(v - \bar{v}) \rangle / (\sigma_v \sigma_\theta)$.

Simulation method

We perform Monte Carlo simulations of a discrete-time correlated random walk process in a two-dimensional square box of size D with periodic boundary conditions. In each simulation, we consider a single hidden target at a random position and a persistent random searcher starting with a random initial position and direction of motion. The target size is chosen to be 1 μm and the results presented in the paper belong to the system size of $D = 250 \mu\text{m}$. We obtain the first-passage time, as the time taken for the searcher to reach the target for the first time. By averaging over an ensemble of 10^5 initial positions and directions, the mean first-passage time τ is

obtained. The algorithm can be extended to multistate stochastic processes [47]. The experimental distribution of speeds $P(v)$ is served as input for simulations. At each step of the simulation, a new instantaneous speed is extracted from $P(v)$ by means of the sum-of-uniforms algorithm [48, 49]— which generates correlated data with a demanded autocorrelation and a certain marginal distribution. In this method, the desired correlations are achieved by allowing a certain degree of stochasticity in the generated data. This algorithm is also used to generate a new direction of motion with a demanded cross-correlation $\mathcal{C}_{\theta-v}$. We systematically vary the θ - v cross-correlation $\mathcal{C}_{\theta-v}$ and autocorrelations \mathcal{AC}_v and \mathcal{AC}_θ and determine the resulting impact on the first-passage properties of the correlated stochastic dynamics.

RESULTS AND DISCUSSION

To better understand the dynamics of migrating immune cells, we consider the motion of immature dendritic cells in 2D *in vitro* experiments. These cells are responsible for antigen capture by tissue patrolling. The natural living environment of immature dendritic cells is interstitial space of peripheral tissues as, for example, the dermal dendritic cells in the skin. We first extract the statistics of instantaneous speeds and orientations from the experimental data, as described in the “Materials and methods” section. Next, we resort to numerical simulations to clarify how the correlated dynamics of cells influences their search abilities.

Cell speed statistics

By analyzing the instantaneous speeds of migrating cells, we deduce the probability distribution of speed, $P(v)$; see Fig. 2. The distribution peaks at small values of v and decays at larger speeds. The mean migration speed is

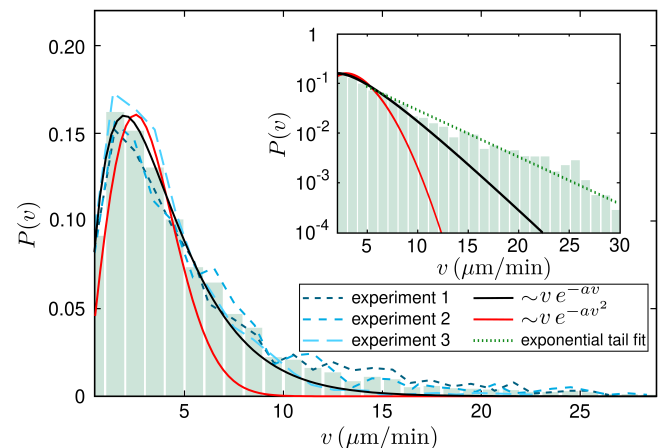


FIG. 2. Probability distribution of speed, $P(v)$, extracted from all cell trajectories. The dashed lines represent $P(v)$ for three independent experiments. The solid lines are overall fits to the given functions. The inset represents the same plot in log-lin scale. The dotted line denotes an exponential fit to the tail of the distribution.

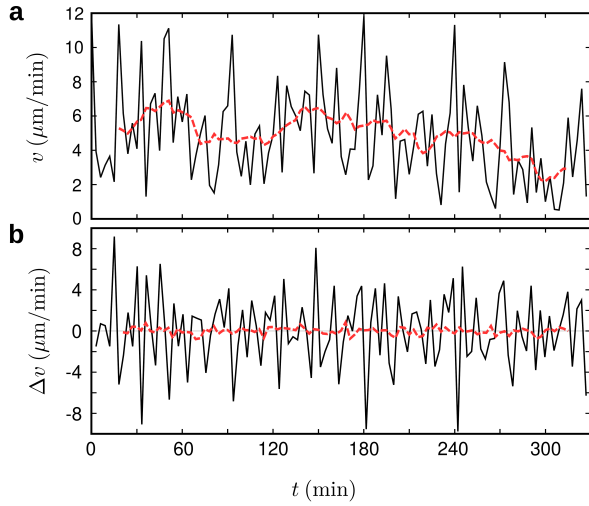


FIG. 3. (a) Example of the instantaneous cell migration speed v over time. The dashed line represents the moving average of v over a 30 min period. (b) Instantaneous speed change Δv over time for the same trajectory as in panel (a). The dashed line is a 30 min moving average of Δv .

$$\langle v \rangle = 5.11 \pm 0.08 \mu\text{m}/\text{min}.$$

While $P(v)$ is expected to follow a Gaussian form in a purely stochastic process, non-Gaussian distributions indicate the presence of memory effects and correlations in the underlying mechanisms of cell migration. Several non-Gaussian forms for the decay of $P(v)$ have been reported in the literature for various cell types—including a slow power-law tail [22], a nearly exponential form [5, 24, 25], and a faster than exponential (but slower than Gaussian) decay [6–8, 23]. Here, we observe a nearly exponential tail, as shown in the inset of Fig. 2. It can be seen that an overall fit to the Maxwell distribution $P(v) \propto v e^{-a v^2}$ (as observed for Hydra cells [23]) or a proposed function $P(v) \propto v e^{-a v}$ for Dicty cells [8] cannot capture the tail behavior of $P(v)$ in our experiments with dendritic immune cells.

The broad distribution of instantaneous speeds evidences that cells should experience considerable speed variations over time. However, $P(v)$ does not contain the necessary information to determine how fast the speed variations occur. One can extract highly correlated data (corresponding to smooth variations of speed) or uncorrelated data (corresponding to abrupt large changes of speed) from the same $P(v)$ distribution in such a way that the distribution of the generated data still follows $P(v)$ [48, 49]. To see the temporal speed changes of cells, successive speeds v and speed changes Δv are presented in Fig. 3 for a typical cell trajectory. The evolution of v is noisy at short timescales. To be able to detect the existing patterns in time, we reduce the noise using a moving average over time. However, choosing a too wide averaging window washes the trends out. Here we have used a 30 min period as a compromise between these two effects, though there is no unique choice for it. The resulting

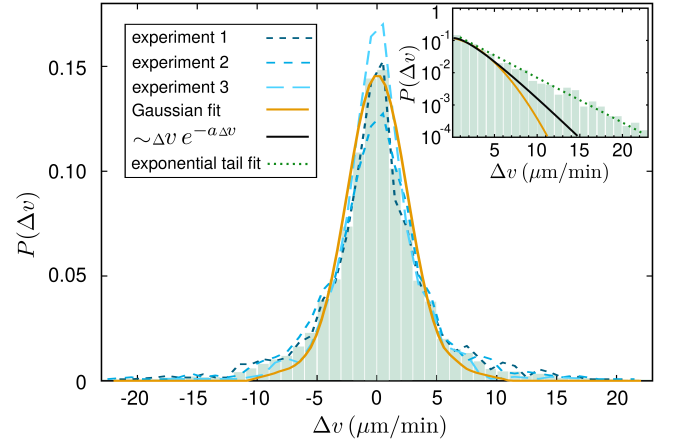


FIG. 4. Probability distribution of instantaneous speed variations, $P(\Delta v)$, for all cell trajectories. The dashed lines represent $P(\Delta v)$ for three independent experiments. The solid line shows an overall Gaussian fit (least square fit, with width and height of the distribution as free parameters). Inset: $P(\Delta v)$ in log-lin scale. The dotted line is an exponential fit to the tail of the distribution.

smoother curve reveals that the cells have the ability to change their speeds smoothly over longer times. This is also reflected in the time evolution of Δv ; although it fluctuates locally, it remains around zero (i.e. the mean speed $\langle v \rangle$) when averaged over a longer time interval of 30 min. To better understand the speed variation statistics, we plot the probability distribution of Δv in Fig. 4. $P(\Delta v)$ develops a sharp peak at zero and decays rather slowly until it diminishes at $|\Delta v| \gtrsim 20 \mu\text{m}/\text{min}$. The tail of $P(\Delta v)$ fits very well to an exponential decay (see inset of Fig. 4); neither a Gaussian function nor an overall fit to $P(\Delta v) \propto \Delta v e^{-a \Delta v}$ can capture the tail behavior.

Speed autocorrelations

Although the data presented in the previous subsection evidences that migrating cells carry a speed memory, as a direct proof we calculate the temporal autocorrelation function of instantaneous speed $\mathcal{AC}_v(t)$, as described in the “Materials and methods” section. Figure 5a shows that there is a rather weak autocorrelation between successive instantaneous speeds. For example, the correlation between two consecutive recorded speeds is $\mathcal{AC}_v \equiv \mathcal{AC}_v(t=3 \text{ min}) = 0.29 \pm 0.03$. $\mathcal{AC}_v(t)$ decays with increasing the time lag t and falls below the noise floor for $t \gtrsim 30 \text{ min}$. We find that the speed autocorrelation function follows a power-law scaling law

$$\mathcal{AC}_v(t) \sim t^{-\beta}, \quad (1)$$

with $\beta = 1.18 \pm 0.03$. Thus, the current migration speed influences the near future speeds, i.e. the cells carry a finite speed memory and change their speed smoothly.

In cell migration studies often the velocity autocorrelation function (VAF) has been reported, which in principle carries information about the diffusivity and path memory of the cell. However, VAF combines the direction and

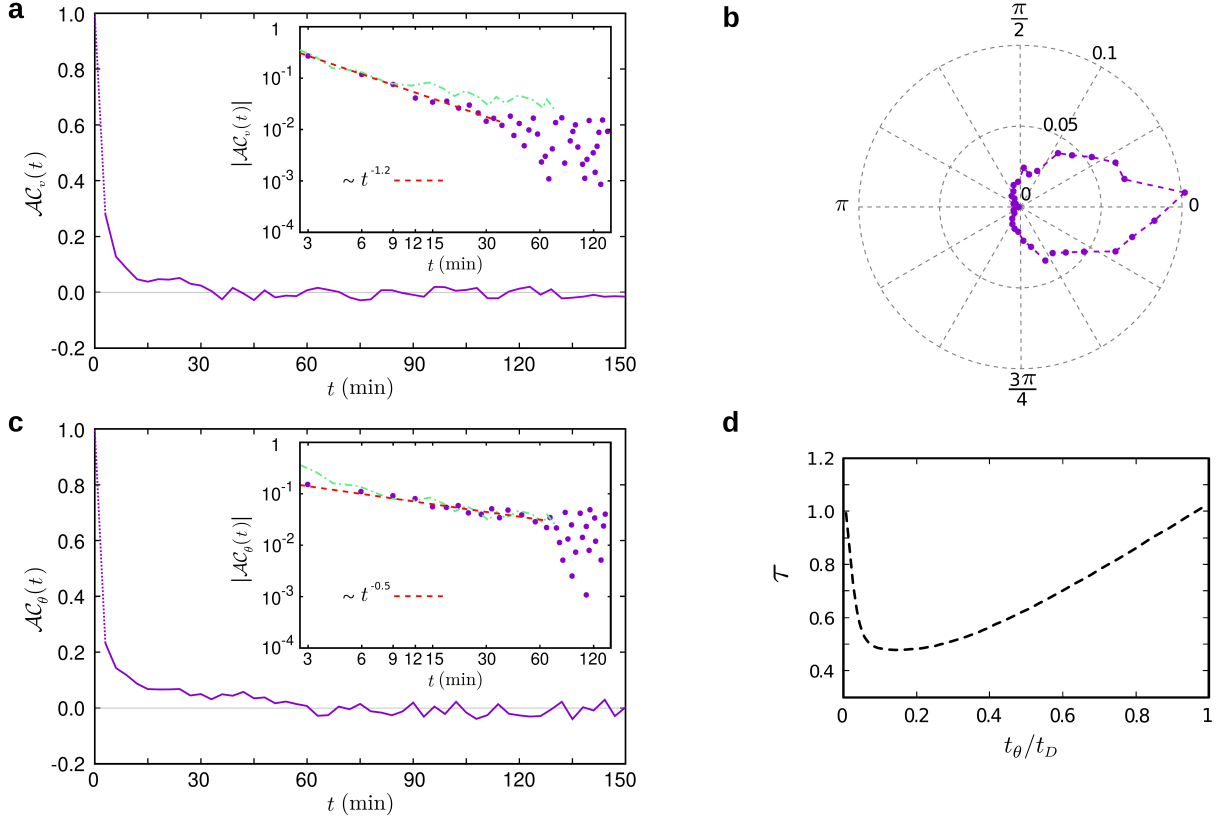


FIG. 5. (a) Temporal autocorrelation function of instantaneous speeds, $\mathcal{AC}_v(t)$. Inset: $|\mathcal{AC}_v(t)|$ in log-log scale. The dashed line represents a power-law fit and the dash-dotted line is the velocity autocorrelation function, VAF. (b) Polar representation of the turning-angle distribution $F(\alpha)$. (c) Temporal autocorrelation function of instantaneous directions, $\mathcal{AC}_\theta(t)$. Inset: $|\mathcal{AC}_\theta(t)|$ in log-log scale. The dashed line represents a power-law fit and the dash-dotted line is the VAF. (d) Mean first-passage time τ (scaled by τ of a non-persistent random walk) in terms of the directional persistence time t_θ (scaled by the timescale t_D to ballistically cross the confinement of size $D = 250 \mu\text{m}$ with a constant speed of $5 \mu\text{m}/\text{min}$).

speed memories of the stochastic process. As a result, one cannot disentangle the contributions of speed and direction variations to the reported diverse behavior of VAF in various types of migrating cells [5–7, 9, 11, 12, 21–24]. Here, we observe that the overall decay of VAF is slower than a power-law (Fig. 5a); it initially decays with a slope which is nearly similar to the slope of $\mathcal{AC}_v(t)$, but the slope gradually reduces at longer times. In the following, we concentrate on the contribution of the directional persistence and compare it to the behavior of the VAF.

Directional persistence

Next we analyze the variations of the cell migration orientation. The local direction of motion with respect to a given (arbitrary) direction in the lab frame can be obtained from every pair of successive recorded positions. Thus, a local direction of motion θ_i is assigned to each recorded position i . The local turning angle is obtained from three successive recorded positions as $\alpha_i = \theta_i - \theta_{i-1}$. Figure 5b shows that the turning-angle distribution $F(\alpha)$ is highly anisotropic with an increased probability for motion in the near forward directions (i.e. $\alpha \approx 0$). We obtain

$\langle \cos \alpha \rangle = 0.51 \pm 0.02$, which has been often used as a dimensionless measure of the directional persistence [50] ($\langle \cos \alpha \rangle$ equals 0 or 1 for diffusion and ballistic motion, respectively).

The directional persistence can be alternatively characterized by the autocorrelation function of cell direction θ . The behavior of the temporal autocorrelation function $\mathcal{AC}_\theta(t)$ of the instantaneous direction, shown in Fig. 5c, has similarities with $\mathcal{AC}_v(t)$; it starts with a moderate value for the minimum lag time $t = 3$ min and decreases with increased time lag t until it falls below the noise floor. However, the striking finding is that the directional autocorrelations last nearly twice longer than the speed autocorrelations (~ 60 vs 30 min). We find that $\mathcal{AC}_\theta(t)$ also follows a power-law scaling

$$\mathcal{AC}_\theta(t) \sim t^{-\gamma}, \quad (2)$$

with $\gamma = 0.51 \pm 0.02$. For comparison, here the correlations are stronger than, e.g., a persistent random walk with constant speed, where the direction autocorrelation function decays exponentially [30]. The smaller power-law exponent for direction autocorrelations compared to the speed data indicates that the directional

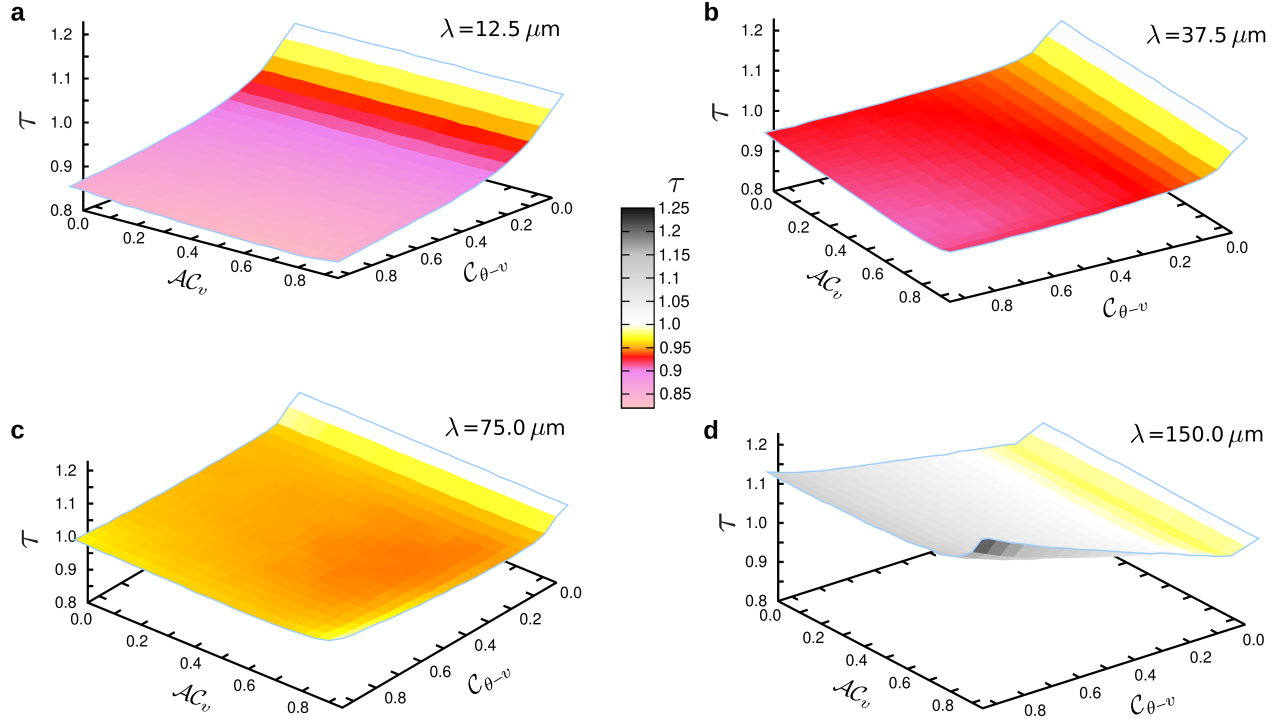


FIG. 6. Mean first-passage time τ in the $(C_{\theta-v}, AC_v)$ space for different values of the mean persistence length λ . τ is given in units of the mean first-passage time of a persistent random walk with the corresponding λ in each panel but with $C_{\theta-v}=AC_v=0$. A simulation box of size $D = 250 \mu\text{m}$ is considered and the results are averaged over an ensemble of 10^5 realizations.

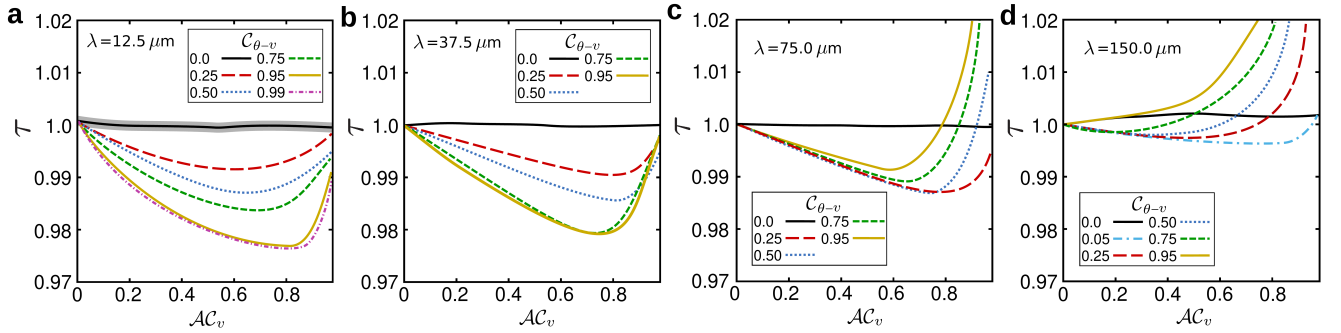


FIG. 7. Mean first-passage time τ in terms of speed autocorrelation AC_v for different values of speed-direction cross-correlation $C_{\theta-v}$. In each panel, the results for a different value of the mean persistence length λ are presented and τ is scaled by its value at $AC_v=0$. The size of the simulation box is $D = 250 \mu\text{m}$. The grey shaded area in panel (a) denotes the standard error for the curve with $C_{\theta-v}=0$, as an example of the typical numerical errors in our simulations.

persistence of the cell can last beyond the timescale that the speed memory is completely lost and the speeds get randomized. It can be seen from Fig. 5c that the VAF initially decays faster than $AC_\theta(t)$ but approaches the slope of $AC_\theta(t)$ at longer times. Together, the insets of Figs. 5a,c suggest that the VAF for our dendritic cells can be roughly fitted by a sum of two power-laws; it follows the behavior of $AC_v(t)$ at short time scales but the behavior is governed by $AC_\theta(t)$ at longer times when the speed memory is lost. Of course, the power-law forms for $AC_\theta(t)$ and $AC_v(t)$ do not necessarily hold for other

migrating cells. Nevertheless, extra information may be extracted in general by decomposing the VAF(t) into $AC_\theta(t)$ and $AC_v(t)$.

There is also a strong cross-correlation $C_{\theta-v}$ between the instantaneous speeds and directions. We obtain $C_{\theta-v} = 0.83 \pm 0.04$ over all cell trajectories; θ and v are dependent variables and the correlated stochastic process can be described by two of the three measures $AC_v(t)$, $AC_\theta(t)$, and $C_{\theta-v}$.

Mean first-passage times

The observed difference between direction and speed

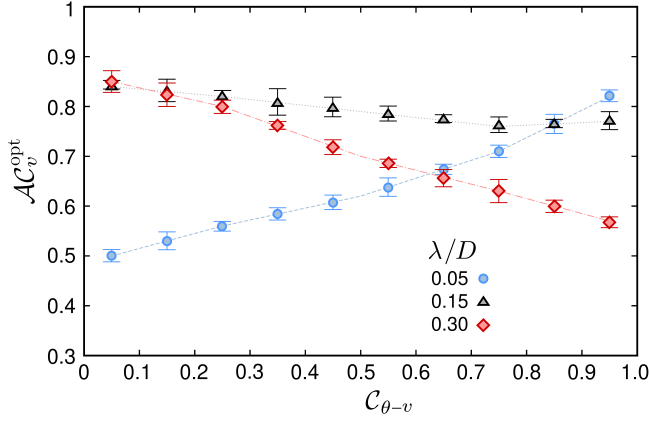


FIG. 8. Optimal speed autocorrelation $\mathcal{AC}_v^{\text{opt}}$ in terms of speed-direction cross-correlation $\mathcal{C}_{\theta-v}$. The results are compared at different values of the mean persistence length λ scaled by the size D of the simulation box.

memories of migrating cells provides an additional degree of freedom, which is expected to influence their navigation and search abilities. We perform extensive Monte Carlo simulations to clarify how cells can benefit from this feature to diversify their search strategies. See the details of the simulation method in the “Materials and methods” section. In the present work we focus on the search problem in the absence of biochemical or other environmental cues to avoid further complications. Thus, we report the numerical results for the problem of finding randomly located targets, which has basic similarities with the task of dendritic immune cells to explore tissues in search for unknown pathogens.

We first study the simpler case of motion with a constant speed but correlated successive directions. The constant speed is set to the mean migration speed of cells, i.e. $v = 5 \mu\text{m}/\text{min}$. The width of the uniform turning-angle distribution $F(\alpha)$ —which is chosen to be symmetric with respect to the incoming direction $\alpha = 0$ —is varied to tune the autocorrelation of directions. From the overall directional persistence $\langle \cos \alpha \rangle$, one can deduce a mean persistence time t_θ since $\langle \cos \alpha \rangle \propto e^{-t_D/t_\theta}$ [51, 52], with t_D being the time required to ballistically cross the confinement of size D . Similarly, a mean persistent length λ can be also deduced (For instance, we obtain $\lambda = 15.3 \pm 0.3 \mu\text{m}$ for our migrating dendritic cells *in vitro*). The mean first-passage time τ to find a randomly located target in the confined area is shown in Fig. 5d in terms of the persistence time t_θ . It can be seen that adopting an optimal directional persistence time t_θ^{opt} minimizes the search time; in large confinements, the achieved reduction compared to a diffusive dynamics can even exceed 50%. This is in agreement with the previous findings that adopting an intermediate directional persistence length optimizes the random search in confinement [14, 41].

While tuning the directional persistence has a strong

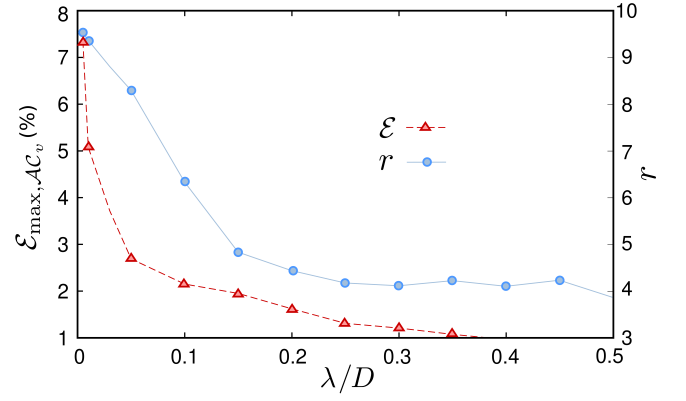


FIG. 9. Maximum attainable search efficiency $\mathcal{E}_{\text{max}, \mathcal{AC}_v}$ by varying \mathcal{AC}_v at a constant value of $\mathcal{C}_{\theta-v}$ (left y-axis) and the ratio r between the maximum attainable search efficiencies upon varying $\mathcal{C}_{\theta-v}$ or \mathcal{AC}_v (right y-axis) versus the relative persistence length λ/D .

impact on τ , the biological agent may not be necessarily able to move with the optimal directional persistence length λ^{opt} due to, e.g., the crowded biological environment in which it performs the search or due to the internal restrictions of the mechanisms of migration. For example, the mean persistence length λ of migrating dendritic cells is well below the optimal choice λ^{opt} [14]. At a given $\lambda (\neq \lambda^{\text{opt}})$, we have previously proven that inducing a cross-correlation between instantaneous directions and speeds can improve the search efficiency [14]. Our findings in the present study suggest that the speed autocorrelation can act as another degree of freedom to improve the search efficiency. To compare the relative impact of $\mathcal{C}_{\theta-v}$ and speed autocorrelations, we perform simulations at different constant values of the mean persistence length λ , and systematically vary $\mathcal{C}_{\theta-v}$ and the degree of correlation between successive instantaneous speeds, characterized by $\mathcal{AC}_v \equiv \mathcal{AC}_v(t = 3 \text{ min})$. We summarize the resulting search times in the $(\mathcal{C}_{\theta-v}, \mathcal{AC}_v)$ phase space at four different choices of λ in Fig. 6: well below (a), slightly below (b), slightly above (c), and well above (d) the absolute optimal persistence length $\lambda^{\text{opt}} \approx 50 \mu\text{m}$. It can be seen that $\mathcal{C}_{\theta-v}$ is a more influential factor than \mathcal{AC}_v in all regimes, especially at small λ . However, there are also considerable variations along the \mathcal{AC}_v axis, which are more pronounced at λ values around λ^{opt} where the dominance of the role of $\mathcal{C}_{\theta-v}$ weakens. For extremely large λ , choosing a $\mathcal{C}_{\theta-v}$ or \mathcal{AC}_v correlated dynamics is disadvantageous and increases τ .

To better understand the influence of \mathcal{AC}_v , we plot τ vs \mathcal{AC}_v for several values of $\mathcal{C}_{\theta-v}$ in Fig. 7. The curves are scaled by τ at $\mathcal{AC}_v = 0$ to highlight the relative variation range of τ upon changing \mathcal{AC}_v . τ reaches a minimum value at an optimal speed autocorrelation $\mathcal{AC}_v^{\text{opt}}$, which depends on the choice of λ and $\mathcal{C}_{\theta-v}$. Figure 8 shows that $\mathcal{AC}_v^{\text{opt}}$ grows with $\mathcal{C}_{\theta-v}$ at small λ regime; thus, a stronger speed autocorrelation is more advantageous at a stronger $\mathcal{C}_{\theta-v}$ coupling in this regime. At $\lambda \sim \lambda^{\text{opt}}$, $\mathcal{AC}_v^{\text{opt}}$ is nearly

independent of the choice of $\mathcal{C}_{\theta-v}$. For $\lambda^{\text{opt}} \ll \lambda$, $\mathcal{AC}_v^{\text{opt}}$ vs $\mathcal{C}_{\theta-v}$ even reverses the direction and monotonically decreases, even though an uncorrelated dynamics performs better in this regime.

The maximum attainable search efficiency via inducing speed autocorrelations depends on the mean persistence length λ ; see the depth of minima in panels (a)-(c) of Fig. 7. To summarize the maximum attainable search efficiency upon increasing the speed autocorrelation, we introduce $\mathcal{E}_{\text{max}, \mathcal{AC}_v}$ as the percentage of reduction in τ at $\mathcal{AC}_v^{\text{opt}}$ compared to τ at $\mathcal{AC}_v = 0$ over all values of $\mathcal{C}_{\theta-v}$. As shown in Fig. 9, $\mathcal{E}_{\text{max}, \mathcal{AC}_v}$ can reach even up to 10% at small values of λ (compared to the confinement size D). This suggests that migrating cells can benefit more from inducing speed autocorrelations in highly crowded environments, where the presence of obstacles lead to very small persistence lengths. The advantage of inducing speed autocorrelations diminishes at persistence lengths $\lambda \gtrsim 0.35 D$. We also note that the role of $\mathcal{C}_{\theta-v}$ is always dominant (compared to \mathcal{AC}_v). By similarly introducing $\mathcal{E}_{\text{max}, \mathcal{C}_{\theta-v}}$ as the percentage of reduction in τ along the $\mathcal{C}_{\theta-v}$ axis over all values of \mathcal{AC}_v , we calculate the ratio $r = \frac{\mathcal{E}_{\text{max}, \mathcal{C}_{\theta-v}}}{\mathcal{E}_{\text{max}, \mathcal{AC}_v}}$ to compare the relative impacts of $\mathcal{C}_{\theta-v}$ and \mathcal{AC}_v on the random search efficiency. Figure 9 reveals that the contribution of $\mathcal{C}_{\theta-v}$ is always more than \mathcal{AC}_v and grows with decreasing λ .

CONCLUDING REMARKS

In summary, we have shown that migrating dendritic cells *in vitro* carry instantaneous speed and direction memories over different timescales. While both speed and direction autocorrelation functions follow power-law decays with time, the later decreases more slowly. These results provide evidence that the cells have different control on their instantaneous speed and direction of motion. We note that the complex *in vivo* conditions— i.e. the combined effects of cell type, crowding, confinement, adhesion (leading to a mixture of different migration modes), presence of environmental cues, etc.— affect the cell dynamics, including their speed and direction autocorrelations, \mathcal{AC}_v and \mathcal{AC}_θ , and the cross-correlation $\mathcal{C}_{\theta-v}$. This can diversify the degree of inequality in the ability of cells to control their speed or persistence. It remains for future studies to understand how the generated biochemical forces and other underlying mechanisms for cell locomotion influence the cell speed and persistence differently.

In numerical simulations, we have clarified the possible impact of each element of the correlated dynamics (i.e. \mathcal{AC}_v , \mathcal{AC}_θ , or $\mathcal{C}_{\theta-v}$) on the efficiency of a persistent stochastic search process to find randomly located targets in confinement. We emphasize that our numerical results and conclusions for navigation strategies and search effi-

ciency of migrating cells are independent of the specific conditions studied in our *in vitro* experiments. While each *in vitro* or *in vivo* experimental condition results in a different set of $(\mathcal{AC}_v, \mathcal{AC}_\theta, \mathcal{C}_{\theta-v})$ values, we have explored the entire range of \mathcal{AC}_v , \mathcal{AC}_θ , and $\mathcal{C}_{\theta-v}$ parameters in simulations. Hence, we have numerically studied every possible type of cell dynamics that can be realized in experiments. This enables us to identify the optimal search strategy for any given experimental condition.

In our experiments, the cells were vertically confined between the parallel plates but the lateral movement was not limited by any pillar for simplicity. While the impact of crowding on cell migration has been studied in similar quasi-2D devices in the presence of a regular array of micropillars [53–57], it is unclear how the correlated dynamics of cells is affected by the obstacles in general. A relevant piece of information, so far, is that increasing the obstacle density reduces the cell persistence [53]. Our numerical results suggest that under a limited variation range of persistence, alternative strategies— i.e. inducing speed autocorrelation or speed-direction cross-correlation—, can be beneficial to improve the search efficiency. Although the latter has a more profound impact, the ability of cells to vary their speeds smoothly can be also advantageous in crowded environments.

Our findings help to better understand the optimality of search and navigation by immune cells and, thus, the underlying mechanisms of the immune response. The results can be also helpful to design efficient navigation strategies for robotics and other technological applications. In the present study, the search problem has been limited to finding randomly located targets. However, similar conclusions can be drawn for correlated stochastic searches in the presence of biochemical or other environmental cues. Our approach offers a framework that allows for quantitative studies of navigation and search problems with correlated dynamics in complex environments.

ACKNOWLEDGEMENTS

We thank Theresa Jakuszeit for fruitful discussions. This work was funded by the Deutsche Forschungsgemeinschaft (DFG) through Collaborative Research Center SFB 1027. M.R.S. acknowledges support by the Young Investigator Grant of the Saarland University, Grant No. 7410110401.

AUTHOR CONTRIBUTIONS

All authors designed and performed research. M.R.S. wrote the manuscript. Correspondence and request for materials should be addressed to M.R.S. (shaebani@lusi.uni-sb.de).

COMPETING FINANCIAL INTERESTS

The authors declare no conflict of interest.

- [2] Paul, C. D., P. Mistriotis, and K. Konstantopoulos. 2017. Cancer cell motility: Lessons from migration in confined spaces. *Nat. Rev. Cancer*. 17:131-140.
- [3] Yamada, K. M., and M. Sixt. 2019. Mechanisms of 3D cell migration. *Nat. Rev. Mol. Cell Biol.* 20:738-752.
- [4] Franco, S. J., and U. Muller. 2011. Extracellular matrix functions during neuronal migration and lamination in the mammalian central nervous system. *Dev. Neurobiol.* 71:889-900.
- [5] Wu, P.-H., A. Giri, S. X. Sun, and D. Wirtz. 2014. Three-dimensional cell migration does not follow a random walk. *Proc. Natl. Acad. Sci. USA*. 111:3949-3954.
- [6] Mitterwallner, G. B., B. C. Schreiber, J. O. Daldrop, J. O. Rädler, and R. R. Netz. 2020. Non-Markovian data-driven modeling of single-cell motility. *Phys. Rev. E*. 101:032408.
- [7] Bödeker, H. U., C. Beta, T. D. Frank, and E. Bodenschatz. 2010. Quantitative analysis of random amoeboid motion. *EPL*. 90:28005.
- [8] Cherstvy, A. G., O. Nagel, C. Beta, and R. Metzler. 2018. Non-Gaussianity, population heterogeneity, and transient superdiffusion in the spreading dynamics of amoeboid cells. *Phys. Chem. Chem. Phys.* 20:23034.
- [9] Harris T. H. *et al.* 2012. Generalized Lévy walks and the role of chemokines in migration of effector CD8+ T cells. *Nature*. 486:545-548.
- [10] Huda S. *et al.* 2018. Lévy-like movement patterns of metastatic cancer cells revealed in microfabricated systems and implicated in vivo. *Nat. Commun.* 9:4539.
- [11] Tee, J. Y., and A. Mackay-Sim. 2021. Directional persistence of cell migration in Schizophrenia patient-derived olfactory cells. *Int. J. Mol. Sci.* 22:9177.
- [12] Nousi, A., M. Tangen Sogaard, M. Audoin, and L. Jaufred. 2021. Single-cell tracking reveals super-spreading brain cancer cells with high persistence. *Biochem. Biophys. Rep.* 28:101120.
- [13] Maiuri P. *et al.* 2015. Actin flows mediate a universal coupling between cell speed and cell persistence. *Cell*. 161:374-386.
- [14] Shaejabi M. R., R. Jose, L. Santen, L. Stankevics, and F. Lautenschläger. 2020. Persistence-speed coupling enhances the search efficiency of migrating immune cells. *Phys. Rev. Lett.* 125:268102.
- [15] Maiuri P. *et al.* 2013. The first world cell race. *Curr. Biol.* 23:97.
- [16] Berg, H. C. 2004. *E. coli in motion*. Springer Verlag, New York.
- [17] Pinkoviezky, I., and N. S. Gov. 2013. Transport dynamics of molecular motors that switch between an active and inactive state. *Phys. Rev. E*. 88:022714.
- [18] Hafner A. E. *et al.* 2016. Run-and-pause dynamics of cytoskeletal motor proteins. *Sci. Rep.* 6:37162.
- [19] Klumpp, S., and R. Lipowsky. 2005. Active diffusion of motor particles. *Phys. Rev. Lett.* 95:268102.
- [20] Höfling, F., and T. Franosch. 2013. Anomalous transport in the crowded world of biological cells. *Rep. Prog. Phys.* 76:046602.
- [21] Dieterich, P., R. Klages, R. Preuss, and A. Schwab. 2008. Anomalous dynamics of cell migration. *Proc. Natl. Acad. Sci. USA*. 105: 459-463.
- [22] Takagi, H., M. J. Sato, T. Yanagida, and M. Ueda. 2008. Functional analysis of spontaneous cell movement under different physiological conditions. *PLOS ONE*. 3:2648.
- [23] Upadhyayaa, A., J.-P. Rieub, J. A. Glazier, and Y. Sawadac. 2001. Anomalous diffusion and non-Gaussian velocity distribution of Hydra cells in cellular aggregates. *Physica A*. 293:549-558.
- [24] Selmecci, D., S. Mosler, P. H. Hagedorn, N. B. Larsen, and H. Flyvbjerg. 2005. Cell motility as persistent random motion: theories from experiments. *Biophys. J.* 89:912-931.
- [25] Czirók, A., K. Schlett, E. Madarász, and T. Vicsek. 1998. Exponential distribution of locomotion activity in cell cultures. *Phys. Rev. Lett.* 81:3038-3041.
- [26] Selmecci D. *et al.* 2008. Cell motility as random motion: A review. *Eur. Phys. J. Spec. Top.* 157:1-15.
- [27] Bénichou, O., C. Loverdo, M. Moreau, and R. Voituriez. 2011. Intermittent search strategies. *Rev. Mod. Phys.* 83:81-129.
- [28] Wadhams, G. H., and J. P. Armitage. 2004. Making sense of it all: bacterial chemotaxis. *Nat. Rev. Mol. Cell Biol.* 5:1024-1037.
- [29] Bartumeus, F., and S. A. Levin. 2008. Fractal reorientation clocks: Linking animal behavior to statistical patterns of search. *Proc. Natl. Acad. Sci. USA*. 105:19072-19077.
- [30] Tierno P., and M. R. Shaejabi. 2016. Enhanced diffusion and anomalous transport of magnetic colloids driven above a two-state flashing potential. *Soft Matter*. 12:3398.
- [31] Sadjadi, Z., and M. R. Shaejabi. 2021. Orientational memory of active particles in multistate non-Markovian processes. *Phys. Rev. E*. 104:054613.
- [32] Jerison, E. R., and S. R. Quake. 2020. Heterogeneous T cell motility behaviors emerge from a coupling between speed and turning in vivo. *eLife* 9:e53933.
- [33] Shaejabi, M. R., L. Stankevics, D. Vesperini, M. Urbanska, D. A. D. Flormann, E. Terriac, A. K. B. Gad, F. Cheng, J. E. Eriksson, and F. Lautenschläger. 2021. Role of vimentin in migration, search efficiency, and mechanical resilience of dendritic cells. Submitted.
- [34] Leithner A. *et al.* 2016. Diversified actin protrusions promote environmental exploration but are dispensable for locomotion of leukocytes. *Nat. Cell Biol.* 18:1253-1259.
- [35] Petrie, R. J., A. D. Doyle, and K. M. Yamada. 2009. Random versus directionally persistent cell migration. *Nat. Rev. Mol. Cell Biol.* 10:538-549.
- [36] Schuss, Z., A. Singer, and D. Holcman. 2007. The narrow escape problem for diffusion in cellular microdomains. *Proc. Natl. Acad. Sci. U.S.A.* 104:16098-16103.
- [37] Bauer, M., and R. Metzler. 2012. Generalized facilitated diffusion model for DNA-binding proteins with search and recognition states. *Biophys. J.* 102:2321-2330.
- [38] Jose R. *et al.* 2018. Trapping in and escape from branched structures of neuronal dendrites. *Biophys. J.* 115:2014-2025.
- [39] Najafi J. *et al.* 2018. Flagellar number governs bacterial spreading and transport efficiency. *Sci. Adv.* 4:eaar6425.
- [40] Oshanin, G., O. Vasilyev, P. L. Krapivsky, and J. Klafter. 2009. Survival of an evasive prey. *Proc. Natl. Acad. Sci. U.S.A.* 106:13696-13701.
- [41] Tejedor, V., R. Voituriez, and O. Bénichou. 2012. Optimizing persistent random searches. *Phys. Rev. Lett.* 108:088103.
- [42] Berre, M. L., E. Zlotek-Zlotkiewicz, D. Bonazzi, F. Lautenschläger, and M. Piel. 2014. Methods for two-dimensional cell confinement. *Methods Cell Biol.* 121:213-229.
- [43] Mohanasundaram P. *et al.* 2022. Cytoskeletal vi-

- mentin regulates cell size and autophagy through mTORC1 signaling, to appear in *Plos Biol.*; bioRxiv: 10.1101/2021.04.19.440145.
- [44] Huang, X., H. Guo, C. Wang, J. Mu, H. Zhang, Z. Liang, J. Cai, and C. Zhou. 2015. Detection of CD28/CD86 co-stimulatory molecules and surface properties of T and dendritic cells: An AFM study. *Scanning*. 38:365-375.
 - [45] Xing, F., J. Wang, M. Hu, Y. Yu, G. Chen, and J. Liu. 2011. Comparison of immature and mature bone marrow-derived dendritic cells by atomic force microscopy. *Nanoscale Res. Lett.* 6:455.
 - [46] Shaebani M. R. *et al.* 2014. Anomalous diffusion of self-propelled particles in directed random environments. *Phys. Rev. E*. 90:030701.
 - [47] Shaebani, M. R., and H. Rieger. 2019. Transient anomalous diffusion in run-and-tumble dynamics. *Front. Phys.* 7:120.
 - [48] Chen, J.-T. 2005. Using the sum-of-uniforms method to generate correlated random variates with certain marginal distribution. *Eur. J. Oper. Res.* 167:226-242.
 - [49] Willemain, R. T., and A. P. Desautels. 1993. A method to generate autocorrelated uniform random numbers. *J. Stat. Comput. Simul.* 45:23-31.
 - [50] Sadjadi Z. *et al.* 2015. Persistent-random-walk approach to anomalous transport of self-propelled particles. *Phys. Rev. E*. 91:062715.
 - [51] Landau, L. D., and E. M. Lifshitz. 1958. *Statistical Physics*. Pergamon Press, Oxford.
 - [52] Doi, M., and S. F. Edwards. 1986. *The Theory of Polymer Dynamics*. Oxford University Press, Oxford.
 - [53] Sadjadi, Z., D. Vesperini, A. M. Laurent, L. Barnefske, E. Terriac, F. Lautenschläger, and H. Rieger. 2022. Amoeboid cell migration through regular arrays of micropillars under confinement. bioRxiv:10.1101/2022.04.08.487483.
 - [54] Wondergem, J. A. J., M. Mytiliniou, F. C. H. de Wit, T. G. A. Reuvers, D. Holcman, and D. Heinrich. 2021. Chemotaxis and topotaxis add vectorially for amoeboid cell migration. *bioRxiv* doi: <https://doi.org/10.1101/735779>.
 - [55] Reversat A. *et al.* 2020. Cellular locomotion using environmental topography. *Nature*. 582:582-585.
 - [56] Gorelashvili, M., M. Emmert, K. F. Hodeck, D. Heinrich. 2014. Amoeboid migration mode adaption in quasi-3D spatial density gradients of varying lattice geometry. *New J. Phys.* 16:075012.
 - [57] Arcizet, D. *et al.* 2012. Contact-controlled amoeboid motility induces dynamic cell trapping in 3D microstructured surfaces. *Soft Matter*. 8:1473-1481.